E. Waxman, Weizmann Institute

Lecture notes for the 2008 SLAC Summer institute:
"Cosmic accelerators"

Topics

I. High energy cosmic rays: key observations, general constraints on possible sources, open questions

II. Gamma-ray bursts as particle accelerators

IIa. Prompt emission and acceleration to high energy: key observations, theoretical model basics, particle acceleration, possible relation to ultra-high energy cosmic-ray production, open questions

IIb. Afterglows and collisionless shocks: theoretical model basics, implications and challenges to the theory of relativistic collisionless shocks

III. Acceleration in large scale structure shocks: particle acceleration and non-thermal emission from large-scale structure shocks, predictions for high energy gamma-ray experiments

** Due to time limitations, high energy neutrino emission from UHECR sources was not covered in these lectures.

Reading

A more detailed discussion of the material covered in the lectures may be found in the papers listed below.

1. Pedagogical reviews of the ultra-high energy cosmic-rays (UHECRs) topic:

Proc. PASCOS 2003: *High energy cosmic-rays*, Pramana-J.Phys. 62, 483 (2004); astro-ph/0310079.

Proc. Nobel Symposium 129: *Neutrino Physics*, Phys. Scripta T121, 147 (2005); astro-ph/0502159.

2. A pedagogical review of gamma-ray burst (GRB) physics:

Supernovae and Gamma-Ray bursters, Lecture Notes in Physics 598, 393 (2003); astro-ph/0303517.

3. A review of the implications of GRB observations to the theory of relativistic collisionless shocks:

Plasma Phys. Control. Fusion 48, B137 (2006); astro-ph/0607353.

4. Particle acceleration and non-thermal emission from collisionless large-scale structure shocks are discussed in the following papers:

Loeb & Waxman 2000, Nature 405, 156.

Keshet et al. 2003, ApJ 585, 128.

Keshet, Waxman & Loeb 2004, ApJ 617, 281.

I. UHECRs: Source constraints

I.1 Key Observations

* The cosmic-ray spectrum extends to $>10^{20}$eV.
* The flux at 10^{20}eV is J~1/100 km^2 yr (2π sr).
* At 10^{19}eV: The spectrum flattens (becomes harder, see fig. 1), and
  The composition changes from heavy to light nuclei (see fig. 2).
* The arrival direction distribution is nearly isotropic above 10^{19}eV.
* The $> 10^{19}$eV energy spectrum is shown in fig. 3, and is discussed below.
* HiRes & Auger each report ~30 CRs above 6x 10^{19}eV, which arrive from different directions (no "repeaters").

I.2 Source distribution, energy production rate and spectrum

* The spectral flattening and composition change at 10^{19}eV suggest that the flux above this energy is dominated by a new source. Since light nuclei of such high energy are not confined by the Galactic magnetic field, the isotropy suggests that the new source is extra-Galactic. Thus, while the flux below 10^{19}eV is likely dominated by Galactic sources of heavy nuclei, the flux at higher energy is most likely dominated by extra-Galactic sources of light nuclei.
* We assume in what follows that the $> 10^{19}$eV particles are protons. This is motivated by (i) the fact that the $> 10^{19}$eV energy spectrum is consistent with an extra-Galactic distribution of proton sources (see below), and (ii) the fact that the likely sources are expected to accelerate primarily protons.
* The rate per unit volume $\mathcal{L}$, at which UHECR sources produce energy in protons of energy ~E_p, is given by $\mathcal{L}(E_p)=4\pi J(E_p)\, E_p/d(E_p)$, where $d(E_p)$ is the maximum distance out to which sources of particles with energy E_p are observed (this follows from the fact that the energy flux received from a solid angle $\Delta\Omega$ is

$$JE_p\Delta\Omega=\int_0^d dr\, r^2\Delta\Omega\frac{\mathcal{L}}{4\pi r^2} \qquad).$$

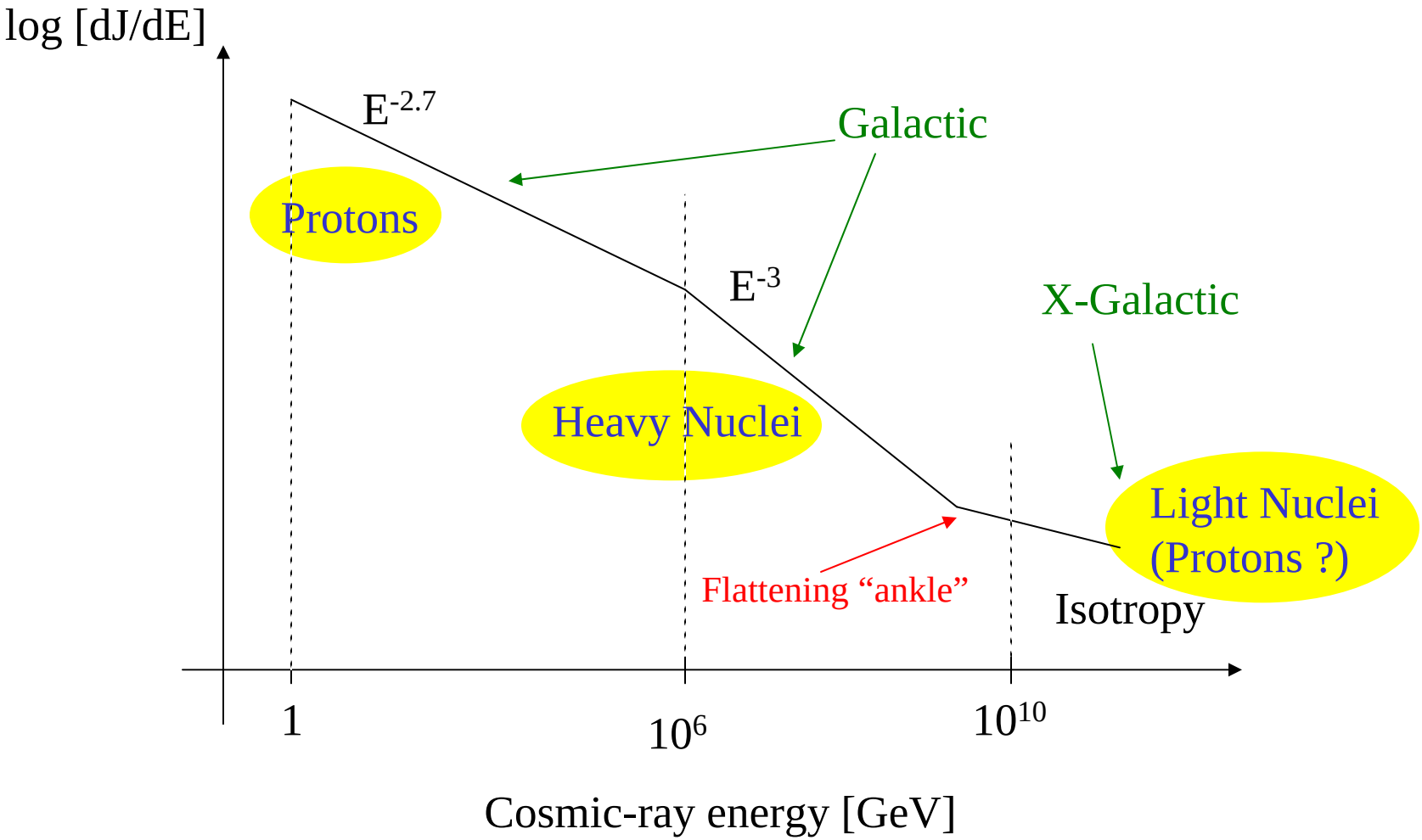

Fig. 1: A schematic description of the differential cosmic-ray number flux, J, as function of energy. The cosmic-ray primary composition at different energies is also indicated.

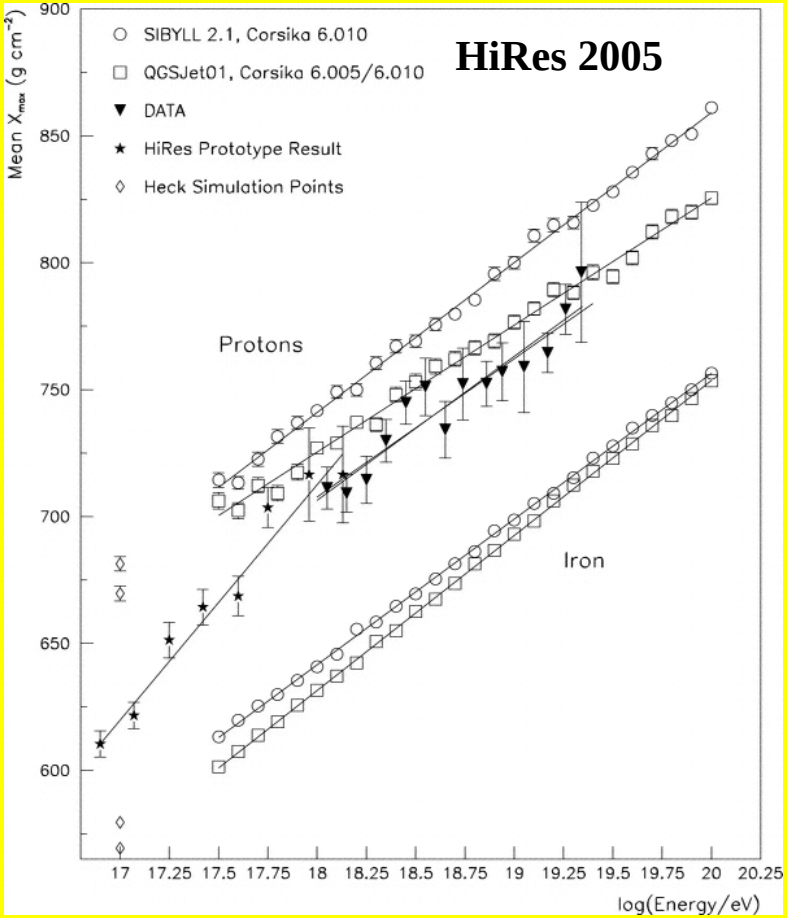

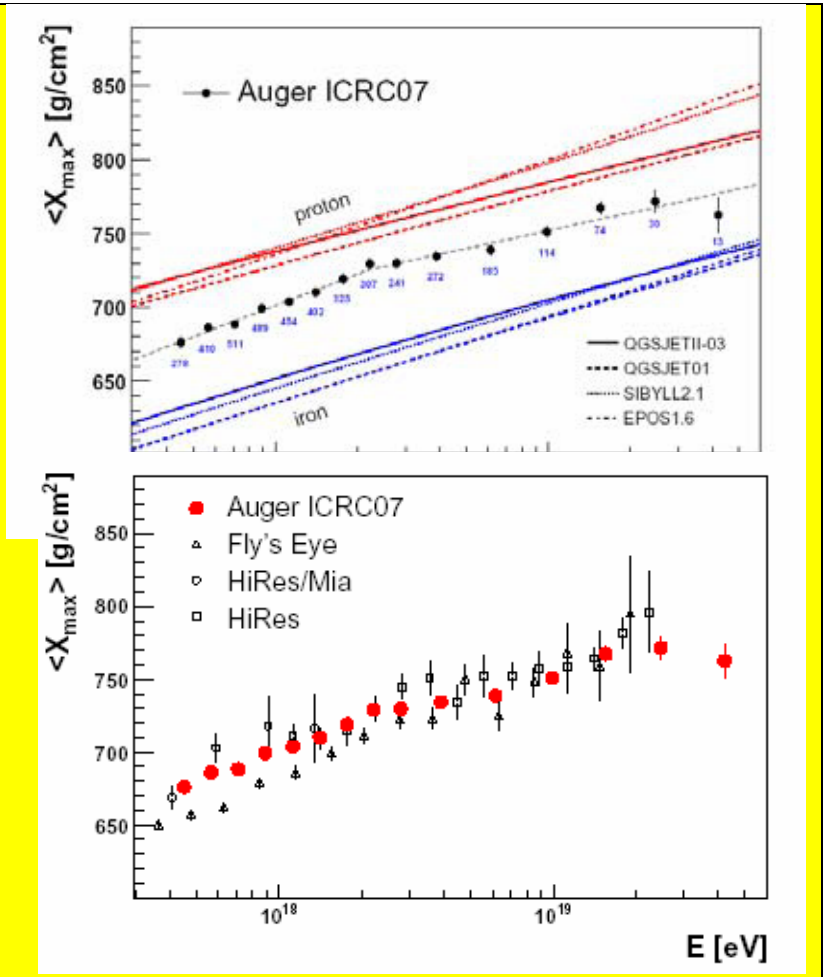

Fig. 2: The energy dependence of the depth in the atmosphere X_{max} at which CR shower maximum is reached. The rapid increase of X_{max} with E below $10^{18.5}$eV [left panel] implies that the composition becomes lighter with E at these energies [the absolute value of X_{max} does not provide a strong constraint on composition, since there is a large uncertainty in the absolute value of X_{max} in the models]. Auger's results are consistent with earlier results [bottom right panel; The claim that the composition becomes heavier again at the highest energies is based on the slight change in X_{max}(E) slope indicated in the top right panel. The validity of this claim is questionable given model uncertainties].

I.2 Source distribution, energy production rate and spectrum (cont'd)

The maximum distance out to which 10^{20}eV proton sources are observed is comparable to the energy loss distance of the protons due to interaction with CMB photons, $p+\gamma \rightarrow N+\pi$. The energy threshold, $E_p E_\gamma > m_p m_\pi c^4$, implies that $E_p = m_p m_\pi c^4/3T_{CMB} = 1.5\times10^{20}$eV protons interact with ~1/2 the CMB photons (note that the CMB spectrum peaks at $3T_{CMB}$=1meV). Since the proton loses a fraction ~m_π/m_p of its energy in a single interaction, we have (n_{CMB}~400/cc, $\sigma_{\gamma p}$~5×10^{-28}cm^2)

$$d(1.5\times10^{20}\text{eV}) \approx \frac{m_p}{m_\pi}\frac{2}{n_{\text{CMB}}\sigma_{\gamma p}} \approx 7\times10^{25}\text{cm} \approx 20\text{Mpc}.$$

10^{20}eV protons interact with a fraction ~0.1 of the CMB photons, thus

$$d(10^{20}\text{eV}) \approx 100\text{Mpc}, \quad \mathcal{L}(10^{20}\text{eV}) \approx \frac{4\pi J(10^{20}\text{eV})\times10^{20}\text{eV}}{d(10^{20}\text{eV})} \approx 0.3\times10^{44}\ \text{erg/Mpc}^3\ \text{yr}.$$

* Fig. 3 shows that the > 10^{19}eV energy spectrum is consistent with an energy independent energy production rate per logarithmic proton energy interval,

$$\mathcal{I}(E_p) = E_p^2(d^3n_p/dVdtdE_p) = 0.6\times10^{44}\ \text{erg/Mpc}^3\ \text{yr}.$$

A uniform energy production per logarithmic proton energy interval is consistent with that expected in collisionless shock acceleration (as discussed at length in L. Drury's lectures).

* As we show below, the deflection of UHECRs due to magnetic fields in the inter-galactic medium is not expected to exceed a few degrees. The detection of 30 CRs above 6x 10^{19}eV from different directions implies therefore that there are >2x30=60 sources out to d(6x 10^{19}eV) (the factor of 2 accounts for the fact that the experiments observe ~1/2 the sky). Using d(6x 10^{19}eV)~200Mpc we find

$$n_{UHECR} > 3\times10^{-6}\ /\text{Mpc}^3.$$

For comparison, the number density of bright galaxies is ~ 3×10^{-3} /Mpc^3.

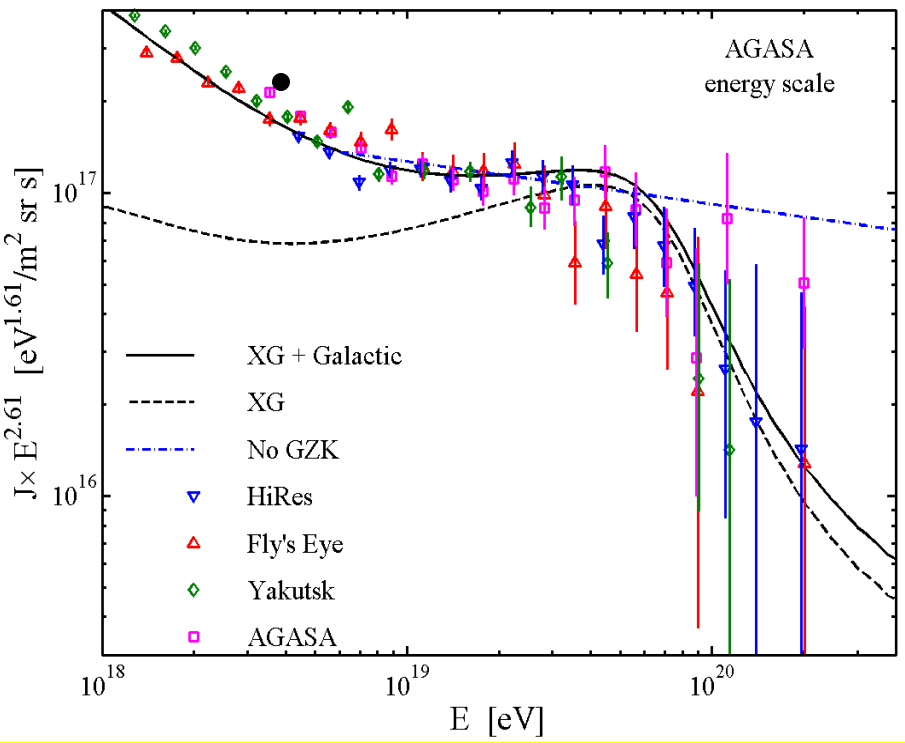

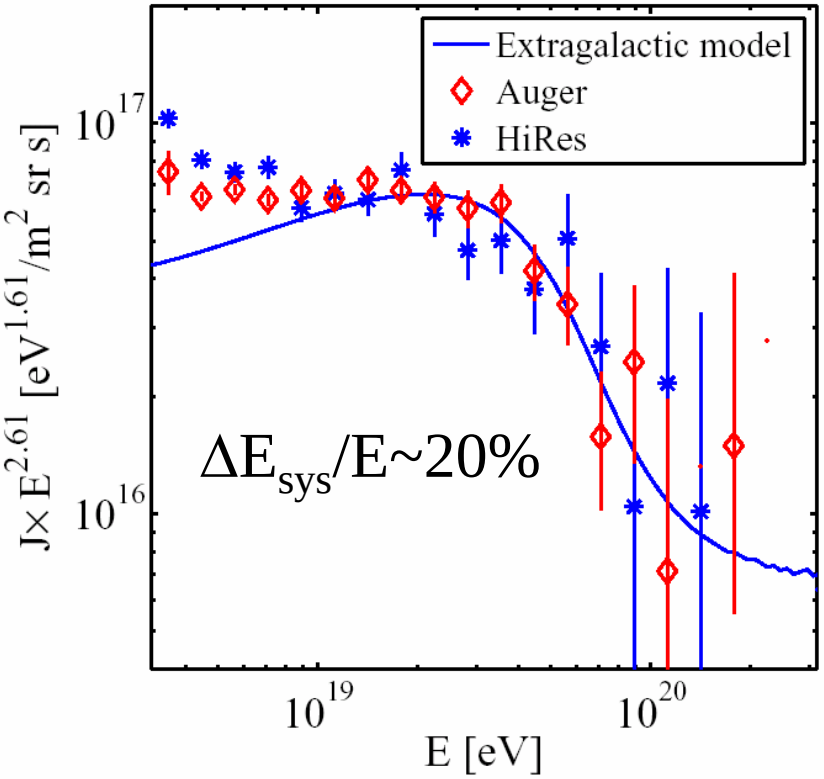

Fig. 3: The observed UHECR spectrum compared to the spectrum predicted in a model where the UHECRs are protons produced by a uniform extra-Galactic distribution of sources, which produce protons with a spectrum $dn_p/dE_p \sim 1/E_p^2$ (equal energy per logarithmic proton energy interval) at a rate $E_p^2 dn_p/dE_p dVdt = 0.6 \times 10^{44} erg/Mpc^3 yr$. The left panel shows pre-Auger data (from Bahcall & Waxman 2003). The dashed curve gives the extra-Galactic model prediction, and the solid curve is obtained by adding the Fly's Eye fit to the Galactic heavy nuclei component (which dominates below 10^{19}eV). The right panel (from Kashti & Waxman 2008) demonstrates that the Auger data are consistent with earlier experiments, after allowing for a systematic under-estimate of the energy of Auger events with respect to HiRes (within the ~25% systematic uncertainty of the UHECR experiments).

I.3 Individual source properties

* Minimum power constraint. Charged cosmic-rays are accelerated in astrophysical sources by electric potentials generated by the motion of magnetized plasma. Consider an astrophysical source driving a flow of magnetized plasma, with characteristic magnetic field strength B and velocity v. Imagine now a conducting wire encircling the source at radius R, as illustrated in fig. 4. The potential generated by the moving plasma is given by the time derivative of the magnetic flux and, as shown in the figure, is therefore given by $V = \beta BR$ where $\beta = v/c$.

If the outflow is relativistic, with Lorentz factor Γ, an accelerated proton can gain only a fraction $1/\Gamma$ of this potential. To see this, one must realize that as the plasma expands, its magnetic field decreases, so the time available for acceleration corresponds to the time of expansion from R to, say, 2R. In the observer frame this time is R/c, while in the plasma rest frame it is $R/\Gamma c$. Thus, a proton moving with the magnetized plasma can be accelerated over a transverse distance R/Γ. This sets a lower limit to the product of the magnetic field and source size, which is required to allow acceleration to E_p,

$$BR > \Gamma E_p/\beta e.$$

This constraint also sets a lower limit to the rate L at which energy should be generated by the source. The magnetic field carries with it an energy density $B^2/8\pi$, and the flow therefore carries with it a power $> 4\pi R^2 v B^2/8\pi$, which implies

$$L > \frac{\Gamma^2}{\beta}\left(\frac{E_p}{10^{20}\,\mathrm{eV}}\right)^2 \times 10^{45.5}\ \mathrm{erg/s} \quad .$$

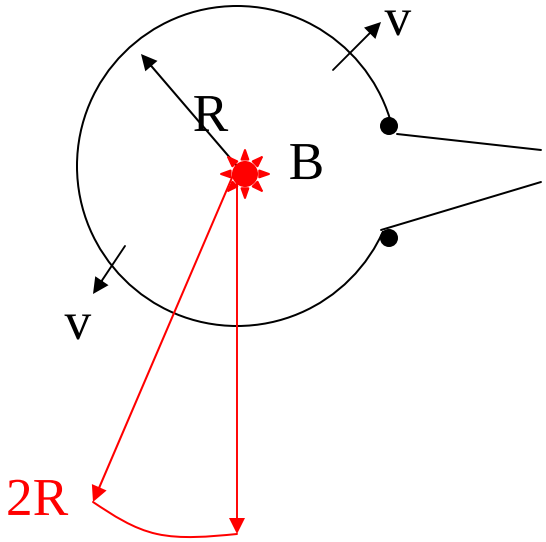

$$V = \frac{1}{c}\dot{\Phi} \sim \frac{1}{c}\frac{BR^2}{R/\mathrm{v}} = \beta BR \quad \Rightarrow \quad \varepsilon_p < \beta eBR/\Gamma$$

$$L > 4\pi R^2 \Gamma^2 \frac{B^2}{8\pi}\mathrm{v} > \frac{1}{2\beta}\left(\frac{\varepsilon_p}{e}\right)^2 c\Gamma^2$$

$$L > 2\frac{\Gamma^2}{\beta}\varepsilon_{p,20}^2 \times 10^{45}\ \mathrm{erg/s}$$

Fig. 4: The minimum power required for proton acceleration to 10^{20}eV.

I.3 Individual source properties (cont'd)

* Minimum Γ constraint. During its acceleration the proton suffers energy losses due to synchrotron emission. Requiring the acceleration time t_{acc} to be smaller than the loss time t_{syn} sets a lower limit to the Lorentz factor. We will assume for simplicity (and then justify) that the flow is mildly or highly relativistic, β~1. t_{acc} (measured in the moving plasma rest frame) may be estimated as the Larmor gyration time, t_{acc}~$2\pi E'_p/eB'c$ (primes denote quantities measured in the plasma rest frame, $E'_p=E_p/\Gamma$), and t_{syn} ~E'_p/P_{syn}, where the synch. power is P_{syn} ~$(m_e/m_p)^2\sigma_T c\gamma_p^2 B'^2/8\pi$ with $\gamma_p=E'_p/m_pc^2$. Assuming that the magnetic field carries a significant fraction of the power, L~$4\pi R^2 c\Gamma^2 B'^2/8\pi$ (the energy density in the observer frame is Γ^2 times the density at the plasma frame), gives

$$B' \sim (L/c)^{1/2}/\Gamma R,$$

and requiring $t_{acc} < t_{syn}$ gives

$$\Gamma^3 R > (m_e/m_p)^2\sigma_T (E_p/m_pc^2)^2 (L/c)^{1/2}/e.$$

As will be shown below in the discussion of GRBs, emission of radiation at radius R by a plasma flowing at speed Γ is expected to produce variability on a time scale $\delta t \sim R/\Gamma^2 c$. Using this relation we finally obtain

$$\Gamma > 1.5 \left(\frac{L}{10^{47}\ \mathrm{erg/s}}\right)^{1/10} \left(\frac{\delta t}{1\mathrm{yr}}\right)^{-1/5} \left(\frac{E_p}{10^{20}\ \mathrm{eV}}\right)^{2/5}.$$

Thus, unless $\delta t \gg 1$yr the flow must be at least mildly relativistic.

I.4 Transient sources

* There is no known steady source that satisfies the power constraint, $L>10^{45.5}\Gamma^2$erg/s, within a distance of several hundred Mpc (recall that $d(E_p=10^{20}eV)\sim100$Mpc). This implies that the sources must be transient. That is, the duration T of their activity should be shorter than the time delay Δt_{CR} in the arrival of cosmic-rays relative to photons. Such time delay may be produced by deflection of CR protons by inter-Galactic magnetic fields.

* The time delay may be estimated as follows. Consider a proton propagating through a magnetic field of characteristic amplitude B and correlation length λ. Assuming that the total deflection is small, over a propagation distance d there are (d/λ) independent deflections of $\delta\theta\sim\lambda/R_L$, where the Larmor radius is $R_L=E_p/eB$. The total deflection is $\theta\sim(d/\lambda)^{1/2}(\lambda/R_L)=(\lambda d)^{1/2}eB/E_p$, and the time delay is $\Delta t_{CR}\sim\theta^2 d/c$. An exact calculation gives

$$\theta=(2\lambda d)^{1/2}eB/3E_p \text{ and } \Delta t_{CR}=\theta^2 d/4c.$$

In part III of the lectures we show that most of the baryons in the present day universe are confined into ~1Mpc diameter filaments, occupying a fraction $f_V\sim0.1$ of the volume with number density ~10 times the universal average and temperature ~0.1keV. Assuming that the magnetic field carries a significant fraction of the thermal energy density of the plasma (an assumption supported by observations, see III), the magnetic field in the filaments is expected to be $B\sim0.01\mu G$. The correlation length of the field may be comparable to (and can not exceed) the largest size of turbulent eddies within the filaments, $\lambda\sim0.1$Mpc. We therefore obtain

$$\theta=(2f_V\lambda d)^{1/2}eB/3E_p\sim1^o(d/100Mpc)^{1/2}(E/10^{20}eV)^{-1},$$

$$\Delta t_{CR}\sim10^{4.5}(d/100Mpc)^2(E/10^{20}eV)^{-2}\ yr=10^{5.5}(d/200Mpc)^2(E/0.6\times10^{20}eV)^{-2}.$$

I.4 Transient sources (cont'd)

* Since $\Delta t_{CR} \sim 1/E^2$, and since there may be multiple paths between the source and the observer, the cosmic rays would be both delayed and spread in arrival time by Δt_{CR}. The effective (i.e. observed) number of CR sources n_{UHECR} is given by

  n_{UHECR}=(transient rate)*Δt_{CR}. Thus, n_{UHECR} is energy dependent.

  In addition, over any given time scale of observation $<<\Delta t_{CR}$, particles of only limited energy range would be observed from a given source. Thus, transient sources are characterized by an apparent narrow spectrum.

* Only two astrophysical sources are known that satisfy $L>10^{45.5}\Gamma^2$erg/s: The brightest steady sources, Active Galactic Nuclei (AGN), and the brightest transient sources, Gamma-Ray Bursts (GRBs). The absence of any known AGN of such high power within several hundred Mpc leaves GRBs as the most likely candidate source. Alternatively, it has been suggested that nearby AGN produce short (T~months) flares of sufficiently high power, $L>10^{46}$erg/s. This possibility can not be ruled out (but such flares have not yet been observed).

I.5 A note on anisotropy

* Since the universe is inhomogeneous on a scales of 100 Mpc, the maximum distance out to which UHECR proton sources are observed, we expect the UHECR arrival direction distribution to show some anisotropy related to this in homogeneity. The left panel of fig. 5 shows the angular dependence of the >6×10^{19}eV CR intensity (normalized to the average, in Galactic coordinates), assuming that the density of UHECR sources is proportional to the galaxy density. The right panel

CR intensity map ($\rho_{source}\sim\rho_{gal}$)

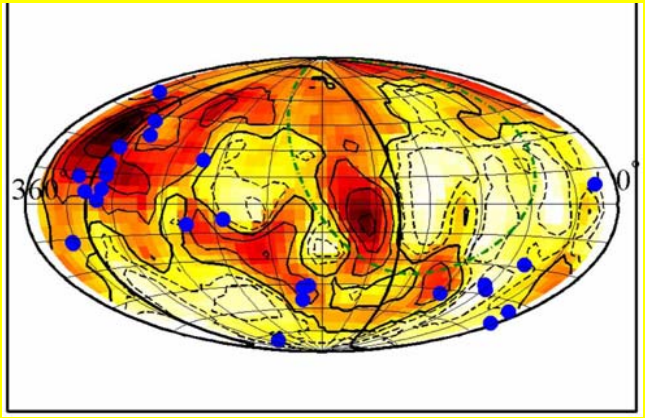

Galaxy density integrated to 75Mpc

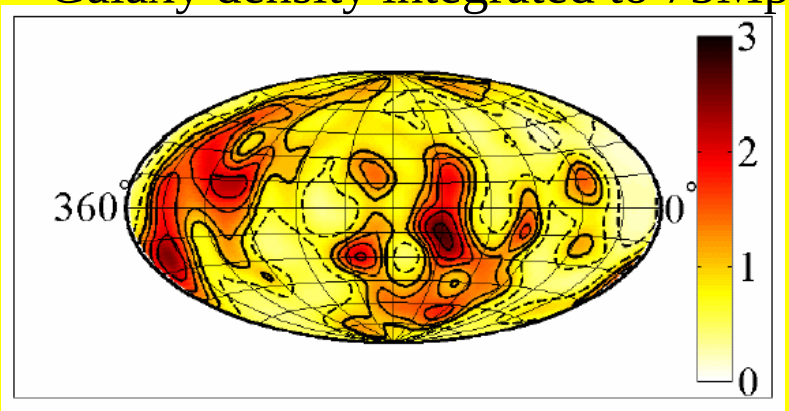

Fig. 5 [from Kashti & Waxman 2008]

shows that the anisotropy pattern clearly reflects the galaxy density distribution. The blue dots are the published Auger >6×10^{19}eV CRs. The observed arrival direction distribution is inconsistent with isotropy at 98% CL, and consistent with the intensity map of the left panel. This gives some additional support to the hypothesis that UHECRs are protons generated by extra-Galactic astrophysical sources.

* The Auger collaboration chose to correlate the >6×10^{19}eV CRs with the VC AGN catalogue, and found a correlation at 99% CL. Does this imply that the sources are AGN? No- the low luminosity AGN in the VC catalogue simply trace the large scale structure (LSS) of the galaxy distribution, so a correlation with them may only suggest a correlation with LSS. So, has the Auger analysis discovered a correlation with LSS? Unfortunately, the answer is again No- The VC catalogue is not uniform and therefore unsuitable for such statistical analysis (see VC paper). The Auger result only indicates (at 99% CL) anisotropy.

A catalogue of quasars and active nuclei: 12th edition⋆

M.-P. Véron-Cetty and P. Véron

Observatoire de Haute Provence, CNRS, 04870 Saint-Michel l'Observatoire, France
e-mail: [mira.veron;philippe.veron]@oamp.fr

Received 9 March 2006 / Accepted 13 April 2006

ABSTRACT

Aims. This catalogue is aimed at presenting a compilation of all known AGN in a compact and convenient form and we hope that it will be useful to all workers in this field.

Methods. Like the eleventh edition, it includes position and redshift as well as photometry (U, B, V) and 6 cm flux densities when and, when available, 20 and 6 cm flux densities.

This catalogue should not be used for any statistical analysis as it is not complete in any sense, except that it is, we hope, a complete survey of the literature.

et al. It contained 202 objects. The number of known quasars has since steadily increased until the year 2000 (see Table 1). The release of both the 2dF catalogue (Croom et al. 2001, 2003) and the first part (Abazajian et al. 2003) of the "Sloan Digital Sky Survey" (Fan et al. 1999) has dramatically increased the number of known quasars justifying the 10th and 11th editions of the present catalogue. The recent release of the last three installments of the SDSS (Abazajian et al. 2004, 2005; Adelman-McCarthy et al. 2006) which has again almost doubled the number of known quasars, made a new edition timely.

This edition contains quasars with measured redshift known to us prior to January 1st, 2006; as in the preceding editions, we do not give any information about absorption lines or X-ray properties. But we give the absolute magnitude[1] for each object and, when available, 20 and 6 cm flux densities.

This catalogue should not be used for any statistical analysis as it is not complete in any sense, except that it is, we hope, a complete survey of the literature.

QSO	BL Lac	Seyfert 1	reference
202			De Veny et al. (1971)
2251		190	Véron-Cetty & Véron (1984)
2835	73	236	Véron-Cetty & Véron (1985)
3473	84	258	Véron-Cetty & Véron (1987)
4169	117	358	Véron-Cetty & Véron (1989)
6225	162	575	Véron-Cetty & Véron (1991)
7383	171	695	Véron-Cetty & Véron (1993)
8609	220	888	Véron-Cetty & Véron (1996a)
11 358	357	1111	Véron-Cetty & Véron (1998)
13 214	462	1711	Véron-Cetty & Véron (2000a)
23 760	608	2765	Véron-Cetty & Véron (2001)
48 921	876	11 777	Véron-Cetty & Véron (2003)
85 221	1122	9628	Present edition

In Table_BL, we list all confirmed, probable or possible BL Lac objects with or without a measured redshift, without consideration of their absolute magnitude. As better spectra are becoming available, broad emission lines have been detected in a

UHECRs- Summary

* $>10^{19}$eV: likely extra-Galactic light nuclei (protons?).

* Energy production rate (per logarithmic proton energy interval) independent of E_p,

  $\mathcal{L}(E_p) = 0.6 \times 10^{44}$ erg/Mpc^3 yr.

* Source density $n_{UHECR} > 3 \times 10^{-6}$ /Mpc^3.

* Source characteristics:

Minimum power	$L > 10^{45.5} (\Gamma^2/\beta)$ erg/s,
Minimum Lorentz factor	$\Gamma > 10^{2.5} (L/10^{52}\ \mathrm{erg/s})^{1/10} (\delta t/10\mathrm{ms})^{-1/5}$,
Transient- duration	$T < 10^{5.5}$ yr,
rate	$>10^{-11}$ /Mpc^{3}yr.

* Candidate sources: GRB
  AGN flares (not yet observed)
  ??

UHECRs- Open Q's

* Composition (nuclei/protons)?
* Source identity?
* Acceleration mechanism?

Potential contributions of large UHECR experiments

* Determine exact spectrum → protons/nuclei?

* Discriminate between steady/transient sources:
  Transient sources have apparent narrow spectrum and
  energy dependent apparent source density.
  For GRBs, only few sources should dominate the flux above $10^{20.5}$eV.

** A significant increase in size beyond Auger may be required to achieve the statistics necessary to test the transient source model predictions.

IIa. GRBs: prompt emission and acceleration to UHE

GRBs are short flashes of MeV photons. Due to time limitations, we will focus here on the class of long duration GRBs. We will assume first that the emission of GRB sources is isotropic, and will later comment on the implications of deviation from spherical symmetry.

IIa.1 Key Observations

* 0.1-2MeV luminosity: $L_{MeV}\sim10^{52}$ erg/s.
* Duration: $T\sim10^{1.5}$ s.
* Rate: ~1000/yr. Since the rate is dominated by the distant, z~1.5, GRBs observed, the z=1.5 implied rate density is $\sim1000/[4\pi(3Gpc)^3/3]\sim10^{-8}/Mpc^3$ yr. The local, z=0, rate is not well constrained. Assuming that the GRB rate evolves like the star-formation, $\sim(1+z)^3$, the z=0 rate density is ~0.5x $10^{-9}/Mpc^3$ yr.
* Variability time: $\delta t\sim10$ms seen in most bursts (that have sufficient photons statistics),
  $\delta t\sim1$ms detected in some (bright) bursts.
* Spectrum: non-thermal, in several cases (bright enough, observed by EGRET/Comptel) extends as $E_\gamma^2(dn_\gamma/dE_\gamma)$=Const. to >100MeV.

IIa.2 Basic theoretical considerations

We give here the basic considerations that lead to the standard "fireball model". A schematic description of the model and the considerations leading to it is given in fig. 6.

* $\delta t\sim1$ms → source radius $R_0<c\delta t\sim10^7$cm; Source mass < $c^2R_0/2G\sim30\ M_{sun}$.
* The energy released, $E_{MeV}=L_{MeV}T\sim10^{53.5}$ erg, is comparable to $M_{sun}c^2$. This, combined with the compact size of the source and its relatively low mass, suggests that the energy source is the collapse of several M_{sun} object to a black hole.

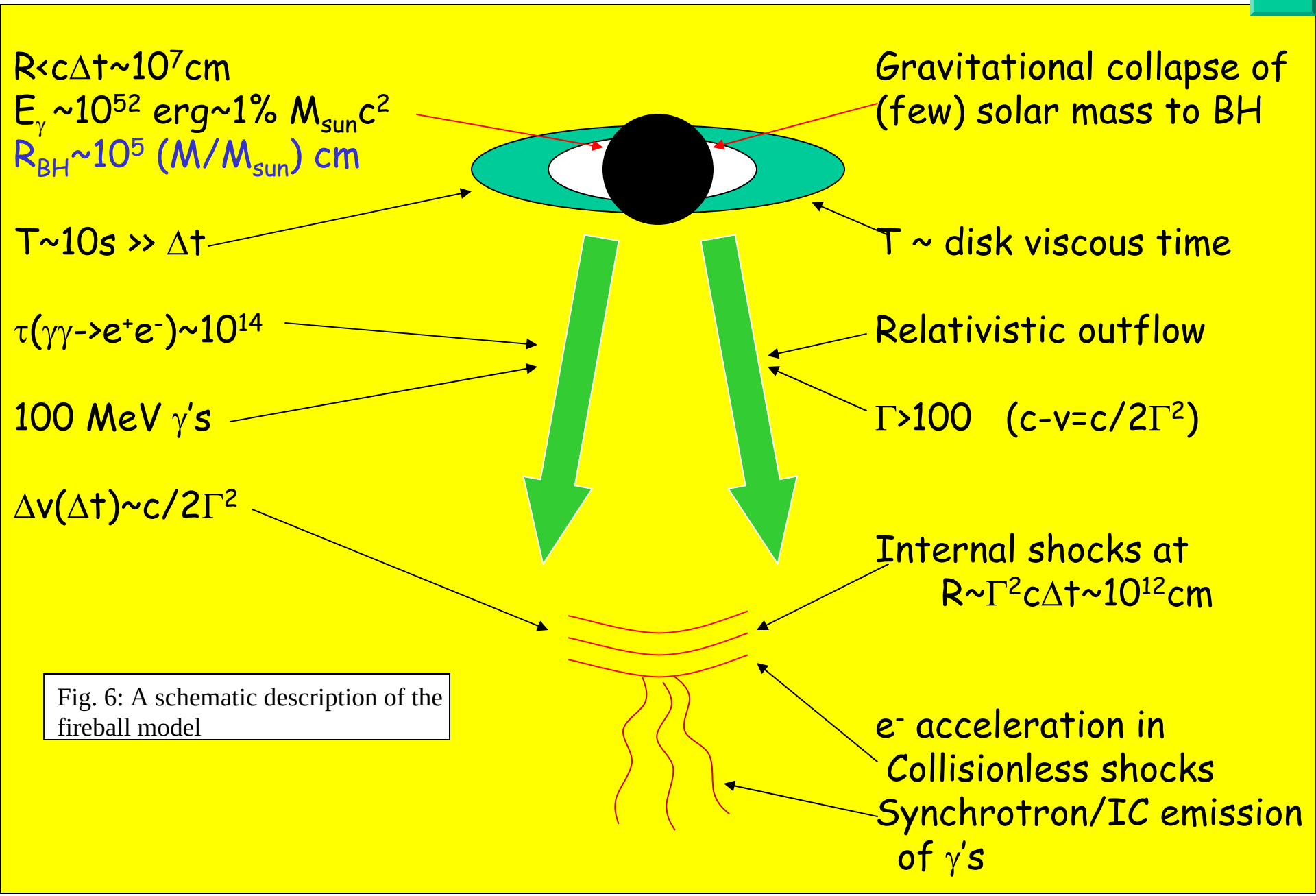

Fig. 6: A schematic description of the fireball model

IIa.2 Basic theoretical considerations (cont'd)

* The burst duration T is much larger than the variability time δt, which is comparable to the collapse time R_0/c. It is therefore believed that the collapse is accompanied by the formation of an accretion disc, which gradually "falls" onto the black hole, releasing the energy on time scale $T \gg \delta t$. The accretion time scale depends on the processes governing angular momentum transport in the disk, which are not well understood.

* For < 30 M_{sun} source, $L > 10^{12} L_{Eddington}$ [$L_{Eddington}=10^{38}(M_s/M_{sun})$erg/s is the luminosity above which the radiation force applied to the plasma exceeds the gravitational binding force] → the plasma emitting the radiation can not be bound to the source, must be out-flowing.

* If the radiation is emitted at $R \sim R_0$, the resulting pair production optical depth is very large:
  $\tau_{\gamma\gamma} \sim n_\gamma \sigma_T R_0$, $n_\gamma \sim L/4\pi R_0^2 c E_\gamma$, $E_\gamma \sim 1$MeV→ $\tau_{\gamma\gamma} \sim 10^{14}$.
  → An optically thick plasma which behaves like a fluid will form, expand and accelerate. This further supports the outflow hypothesis.

* Assume that radiation is produced once the plasma accelerated to Lorentz factor Γ and reached a radius R. R and Γ are constrained by the observed δt. Photons emitted from plasma moving at angle θ with respect to the line of sight are delayed (see fig.) by $\Delta/c = \theta^2 R/c$; Due to relativistic beaming

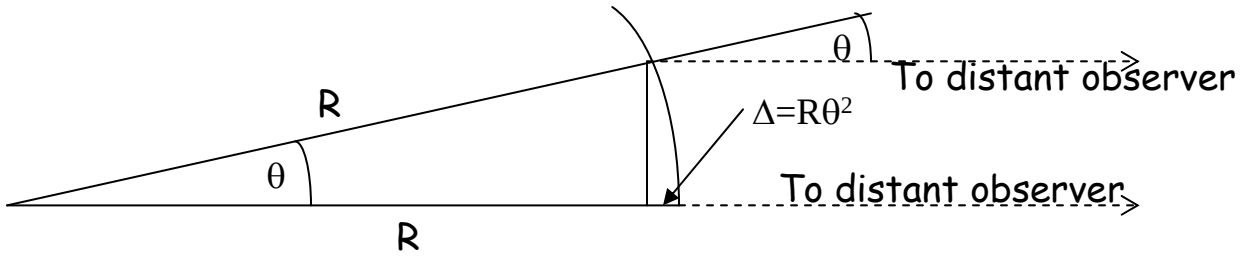

radiation is emitted within a cone of opening angle $1/\Gamma$ around the expansion direction, and therefore reach the observer only from angles $\theta < 1/\Gamma$. A pulse emitted at radius R is therefore spread over $R/\Gamma^2 c$, which requires $R < \Gamma^2 c\, \delta t$.

IIa.2 Basic theoretical considerations (cont'd)

*A lower limit on Γ is set by requiring the pair-production optical depth to be smaller than 1 for the observed E_γ=100MeV photons. This optical depth is given by the product of the interaction rate of photons in the plasma frame, $n_\gamma \sigma_T c$, and the plasma expansion time, $R/\Gamma c$ (in the observer frame this time is R/c, while in the plasma rest frame it is $R/\Gamma c$). n_γ is the number density of photons in the plasma frame with energy exceeding the pair production threshold, $\sim (m_e c^2)^2/(E_\gamma/\Gamma)$ (the plasma frame energy of a photon is smaller by a factor $1/\Gamma$ compared to the observer frame energy). Thus,

$$\tau_{\gamma\gamma}(E_\gamma) \approx n_\gamma \sigma_T c \frac{R}{\Gamma c} \approx \frac{u_\gamma}{\Gamma (m_e c^2)^2 / E_\gamma} \sigma_T \frac{R}{\Gamma}$$

$$\approx \frac{L_{MeV}}{4\pi R^2 \Gamma^2 c} \frac{E_\gamma}{\Gamma (m_e c^2)^2} \sigma_T \frac{R}{\Gamma} = \frac{\sigma_T L_{MeV}}{4\pi R \Gamma^4 c} \frac{E_\gamma}{(m_e c^2)^2} \quad .$$

Here we have estimated the photon energy density in the plasma frame by $u_\gamma \sim L/4\pi\Gamma^2 R^2 c$ (the energy density in the observer frame is larger by a factor Γ^2), and assumed that the energy density per logarithmic photon energy interval is independent of photon energy (and equal to L_{MeV}). Using $R<\Gamma^2 c\,\delta t$ we finally find that $\tau_{\gamma\gamma}<1$ implies

$$\Gamma > \left[\frac{\sigma_T L_{MeV}}{4\pi c^2 \delta t} \frac{E_\gamma}{(m_e c^2)^2} \right]^{1/6} = 10^{2.5} \left(\frac{L_{MeV}}{10^{52}\,\mathrm{erg/s}} \frac{10\mathrm{ms}}{\delta t} \frac{E_\gamma}{100\mathrm{MeV}} \right)^{1/6} .$$

* The preceding discussion suggests that the energy is carried from the "engine", the accreting black hole, by some "wind" of duration T, which varies on time scale δt. A significant fraction of the energy carried by the wind is somehow radiated as MeV photons at a large radius, $R \gg R_0$. There are two generic types of models for the wind: A wind where the energy flux is purely electromagnetic, and a wind where the energy flux is dominated by the kinetic energy of the plasma. The nature of the wind depends on the process converting the gravitational energy released by accretion to plasma outflow energy, which is not well understood.

* In the case of an electromagnetic wind, the process that leads to the emission of radiation at large radius R is not well understood. In the case of a kinetic wind, which is adopted in the common "fireball" model, there is a model that may account for the observed radiation. This model too

faces theoretical challenges, as will be discussed below (IIb).

* In a kinetic wind model, the kinetic energy is naturally expected to be partially dissipated, i.e. converted to heat, at a radius $R=\Gamma^2 c\,\delta t$. The wind properties are expected to fluctuate on a time scale δt. In particular, the Lorentz factor is expected to fluctuate around its mean over this time scale. Faster parts of the flow will therefore overtake slower parts, producing "internal" shocks that dissipate energy, at a distance $R=c*c\delta t/\delta v$, where δv is the characteristic velocity fluctuation. Since for $\Gamma>>1$ we have $v/c=1-1/2\Gamma^2$, $\delta v/c\sim 1/\Gamma^2$ and $R\sim\Gamma^2 c\delta t$.

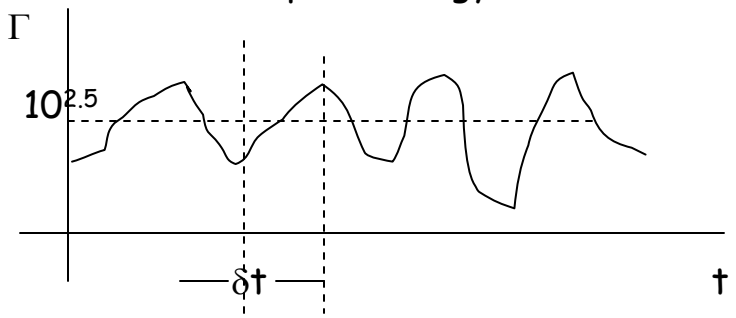

The relative velocities of the different parts of the flow (measured in the average velocity frame of the wind) are expected to be mildly, but not highly, relativistic. This is easy to understand by noting that in the rest frame of two equal masses moving (in the same direction in the observer frame) with $\Gamma_1 > \Gamma_2$, the Lorentz factor of the two masses is $(\Gamma_1 / \Gamma_2)^{1/2}$. Thus, only extreme Γ_1 / Γ_2 ratios can lead to highly relativistic relative motion.

Mildly relativistic relative motion implies that protons will be heated in the shocks to ~1GeV. Since the shocks are collisionless we expect generation of strong magnetic fields (see discussion in IIb). If the electrons are coupled to the protons, and heated to ~1GeV as well, they will emit synchrotron radiation. The characteristic synch. photon energy, in the plasma frame, will be $E'_\gamma \sim h\gamma_e^2 (eB'/2\pi m_e c)$, where B' is the (plasma frame) field and $\gamma_e=m_p/m_e$ is the electron Lorentz factor . If a significant fraction of the energy is carried by the magnetic field then $B' \sim (L/c)^{1/2}/\Gamma R$ (see I.3), and the observed photon energy, $E_\gamma=\Gamma E'_\gamma$ is

$$h\nu_{synch.} \approx 0.5\left(\frac{L_{MeV}}{10^{52}\,\mathrm{erg/s}}\right)^{1/2}\left(\frac{\delta t}{10\mathrm{ms}}\right)^{-1}\left(\frac{\Gamma}{300}\right)^{-2}\ \mathrm{MeV}.$$

The fact that for the obserevd L and δt the model photon energy is consistent with the observed one provides some support for the model.

IIa.2 Basic theoretical considerations (cont'd)

As discussed in L. Drury's lectures, and also below (IIb), collisionless shocks are expected to produce a non-thermal electron distribution, with $\gamma_e^2 dn_e/d\gamma_e$~Const. Such an electron spectrum will produce a non-thermal photon spectrum $E_\gamma^2(dn_\gamma/dE_\gamma)$=Const, as observed (it is straight forward to verify that electrons lose all their energy to radiation on a time scale << plasma expansion time=$R/\Gamma c$.)

* Let us now comment on the assumption of spherical symmetry. We have evidence from afterglow observations (see IIb) that the outflow is not spherical but rather jet-like, with an opening angle θ_j~0.1. This does not modify, however the analysis presented above. First, a jet behaves as if it were a part of a complete sphere as long as $\theta > 1/\Gamma$. This is due to the fact that expansion to radius R takes a time $R/\Gamma c$ in the plasma frame, which implies that signals propagating from the jet center to its edge can reach only an angle $1/\Gamma < \theta$. Second, since the emitted radiation is confined to an angle $1/\Gamma$ around the outflow direction, a distant observer can not observe the "edge" of the jet (unless his line of sight is closer to the edge than $1/\Gamma$).

  The analysis presented above holds therefore for both spherical and conical (jet-like) outflows. In the case of a jet-like out flow, L in the above eqs. should be interpreted as the "isotropic equivalent" power. The true energy of a jet-like out flow is smaller, of course, than the inferred isotropic equivalent energy by a factor $\sim\theta_j^2/2$~0.005 (the true rate is larger by the inverse factor). Thus, the true energy is $E_{MeV,true}$~10^{51}erg (instead of $10^{53.5}$erg). This makes the scenario of a collapse of a few solar mass object to a BH more plausible, since it requires only ~1% of the energy to be released as high energy radiation (it is difficult to see how a much larger fraction could be achieved).

* In order to achieve Lorentz factor Γ, the mass entrained in the expanding wind can not exceed $(\theta_j^2/2)\, E_{MeV,true}/\Gamma c^2 \sim 10^{-6}\ M_{Sun}$. This is a major challenge to the models, given that the mass of the collapsing object is probably ~10 M_{Sun}. This challenge may be more severe for the pure electromagnetic wind models, which require still much smaller entrained mass.

IIa.3 GRBs and UHECRs

The general constraints derived in I on the properties of UHECR sources are compared below to the properties of GRB sources derived in IIa.2 from 1—100MeV photon observations.

	UHECR source constraints	GRB source properties
Energy production rate	$\mathcal{L}_p = 0.6\times10^{44}$ erg/Mpc^3 yr	$\mathcal{L}_e = 10^{44}$ erg/Mpc^3 yr
Minimum power	$L > 10^{50.5}(\Gamma/300)^2$erg/s	Γ=300, $L = 10^{52}$ erg/s
Minimum Lorentz factor	$\Gamma > 10^{2.5}(L/10^{52}\,\mathrm{erg/s})^{1/10}(\delta t/10\mathrm{ms})^{-1/5}$	$\Gamma > 10^{2.5}(L/10^{52}\,\mathrm{erg/s})^{1/6}(\delta t/10\mathrm{ms})^{-1/6}$
Transient duration	$T < 10^{5.5}$ yr,	T=30s
Transient rate	$>10^{-11}$ /Mpc^{3}yr	0.5×10^{-9} /Mpc^{3}yr

Table 1: GRB sources satisfy all the constraints that UHECR sources should satisfy

A few comments:

1. The energy production rate is per logarithmic particle energy interval. For UHECRs- see I.2. For GRBs, the (z=0) luminosity in 0.1-2MeV photons, $\mathcal{L}_{MeV}\sim10^{52}$ erg/s x 30s x 0.5×10^{-9} /Mpc^{3}yr = 10^{44} erg/Mpc^3 yr, reflects the energy deposited in ~1/2 a decade of electron energy ($\nu_{synch}\sim\gamma_e^2$).
2. The numbers given for GRBs (L, rate) are the "isotropic equivalent" ones, not corrected for the GRB outflow being "beamed", i.e. jet-like, instead of spherical. As explained in IIa.2, beaming does not affect the value of $\mathcal{L}_e$ and a jet behaves exactly as if it were a part of a spherical outflow. The GRB rate relevant for the effective number density of UHECR sources is the rate not corrected for beaming, since the typical deflection of UHECRs, ~0.02rad (I.4), is smaller than the typical jet opening angle, ~0.1rad.
3. It is important to emphasize that the 2 constraints on Γ are from completely independent arguments (energy loss of protons for the UHECR constraint, pair optical depth for GRB constraint).

IIb. GRBs: afterglows and collisionless shocks

Due to time limitations, we will discuss here only the key implications of afterglow observations to collisionless shock physics.

IIb.1 Dynamics

* As the fireball plasma expands, it drives a relativistic shock into the surrounding plasma (e.g. into the ISM, the inter-stellar medium). After the shock expands to sufficiently large radius, the flow no longer "remebers" the length scales of the initial conditions, and it approaches the self-similar solutions of Blandford & McKee, which are determined by the total energy deposited into the medium E, and the pre-shock density n.

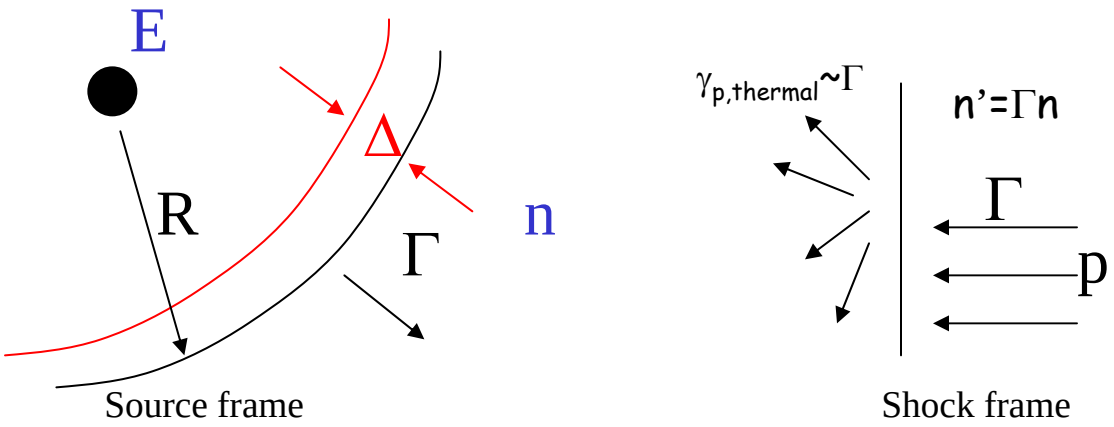

* In the shock frame, the protons flowing with Lorenz factor Γ into the shock are scattered at the shock, so that their post-shock thermal Lorentz factor is $\sim\Gamma$. Boosting back to the source frame, each proton now has an energy of $\Gamma^2 m_p c^2$, so energy conservation implies $E=\Gamma^2 M(R) c^2$ where M(R) is the mass enclosed within R.
* As in the case of prompt emission, radiation emitted from the shock at radius R is observed by a distant observer at $t_{obs}=R/\Gamma^2 c$. For constant n we have $t\sim R^4$.
* Since the expansion time to radius R in the plasma frame is $R/\Gamma c$, the shocked plasma is compressed into a shell of thickness R/Γ in the plasma frame, and R/Γ^2 in the source frame.
* Since a distant observer receives radiation from a cone of opening angle $1/\Gamma$ around the line of sight, the apparent size of the source is $h=R/\Gamma\sim t^{5/8}$.

IIb.1 Dynamics (cont'd)

The predicted apparent source size is

$$h=\frac{R}{2\Gamma}=2\Gamma ct_{\rm obs}=10^{17}\left(\frac{E_{53}}{n_0}\right)^{1/8} t_{\rm week}^{5/8}\,{\rm cm}\quad .$$

Although the angular size of such a source at cosmological distance is exceedingly small, 10^{-11} rad, it was measured directly in two cases. The left panel shows the log of the flux ratio at 5 and 9 GHz radio emission of the "afterglow" following the prompt GRB970508 emission. The strong variations in flux ratio at early times are due to "diffractive scintillation" (see fig. 7), the suppression of which at 40d implies that the source size exceeded few$\times 10^{17}$cm at this time. The right panel shows the radio image of the afterglow of the relatively nearby GRB030329, resovled by large baseline interpherometry (VLBA+Bonn) at 22GHz. The angular size, 0.08mas, corresponds to h(24 days)= 3$\times 10^{17}$cm.

The predicted size depends only weakly on E & n, and therefore provides a stringent test of the model dynamics. As illustrated in the figures, the observed size is consistent with model predictions.

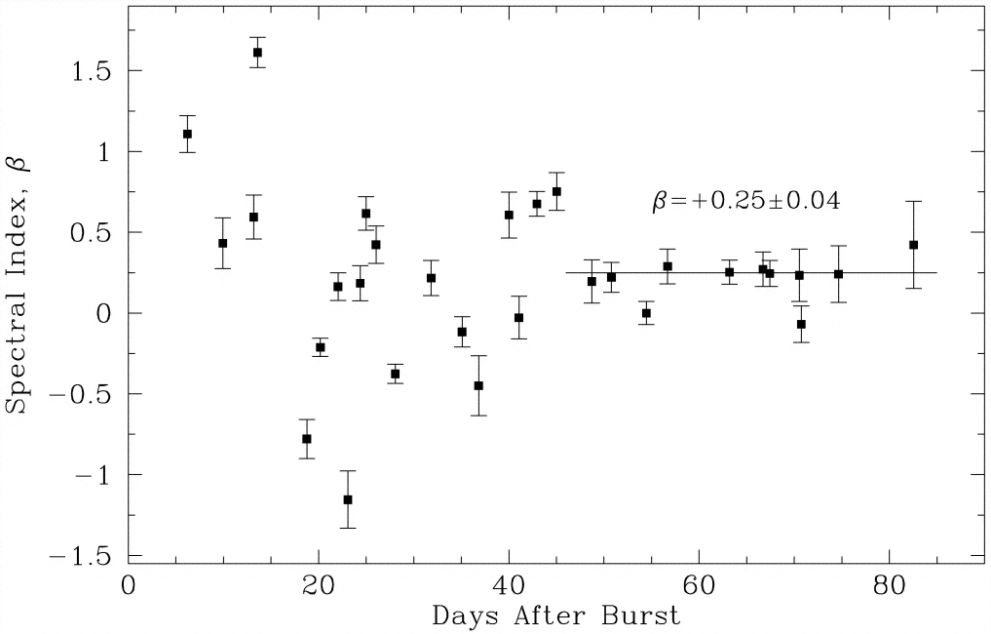

[From: Frail, Waxman & Kulkarni 00]

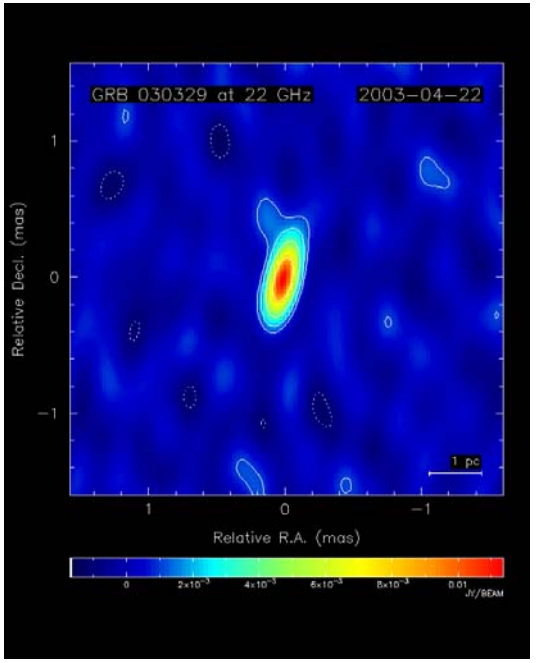

[From: Taylor et al. 03]

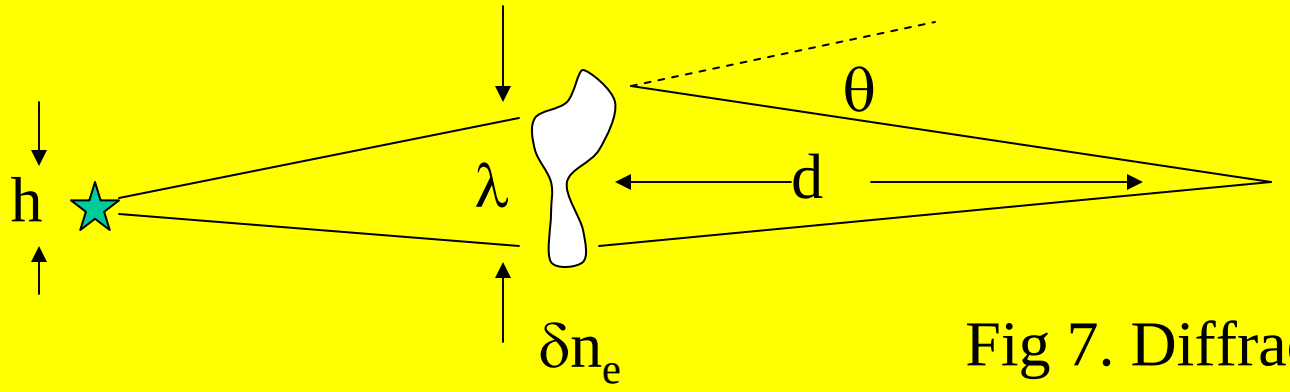

Fig 7. Diffractive scintillation

Radio waves emitted by the source are scattered by inhomogeneities in the electron density in the Galactic ISM. If the deflection angle is large enough, $\theta > \lambda / d$ where λ is the correlation length of density fluctuations, multiple paths between the source and the observer are possible, and a diffraction pattern is formed. In this case, the radio flux will greatly vary as the Earth moves through the ISM. Since deflection is freq. dependent, the diffraction pattern changes rapidly with freq., and variations at nearby freq. are not correlated.

If the source is finite, different points on the source produce different diffraction patterns. If the source is too large, these patterns do not overlap and no large variations in flux will be observed. For a source at cosmological distance, the critical size h beyond which diffractive scintillation is suppressed is h=fewx10^{17}cm.

IIb.2 Collisionless shocks & Radiation

* In lab/atmospheric shocks the process that scatters particles and converts kinetic to thermal energy at the shock transition layer is commonly binary Coulomb collisions. As illustrated in the figure, the thickness of such a shock, which is comparable to the mfp for large deflection Coulomb collisions, is larger than the Hubble size for the low densities characteristic of the ISM. At such low densities, collective plasma effects are dominant. Highly anisotropic particle distributions lead to the development of electro-magnetic instabilities. These develop at a rate comparable to the plasma freq., ω_p, leading to shock thickness ~c/ω_p.

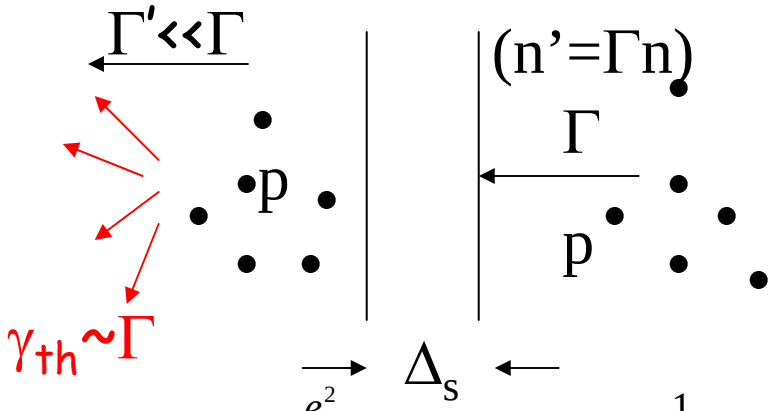

$$\text{Coulomb}: \Gamma m_p c^2 = \frac{e^2}{d} \Rightarrow \Delta_s \sim \lambda_{Coul.} \approx \frac{1}{\Gamma n \pi d^2} = 10^{31}\,\Gamma \left(\frac{n}{1/\text{cm}^3}\right)^{-1} \text{cm}$$

$$\text{Plasma}: \omega_p = \sqrt{\frac{4\pi \Gamma n e^2}{\Gamma m_p}} \Rightarrow \quad \Delta_s \sim \lambda_{sd} = \frac{c}{\omega_p} \approx 10^7 \left(\frac{n}{1/\text{cm}^3}\right)^{-1/2} \text{cm}$$

The development of EM instabilities implies generation of B field, and the absence of Coulomb collisions implies a non-thermal particle distribution at the downstream. This combination implies that synch. emission could be expected. However, no first principles theory exists of the processes of magnetic field generation and non-thermal particle acceleration (and hence of the emission of radiation).

* GRB afterglow emission, generated by the expanding shock, can be explained adopting 3 assumptions:

  1. The magnetic field carries a significant fraction of the post-shock energy density;
  2. The electrons carry a significant fraction of the post-shock energy density;
  3. The electron energy distribution has a high energy tail $\gamma_e^2 dn_e/d\gamma_e$~Const.

  As discussed in detail by L. Drury, we have strong theoretical and observational indications (although no self-consistent theory) that collisionless shocks generate $\gamma^2 dn/d\gamma$~Const particle distributions. We also have strong theoretical indications (both analytic and numeric), that

IIb.2 Collisionless shocks & Radiation (cont'd)

EM instabilities saturate only when the magnetic field carries a significant fraction of the energy density. The two main challenges are:

the coupling of electrons and protons (leading to near equipartition), and

the survival of B over large scale.

Let us discuss the latter challenge in some detail.

* The magnetic field generated at the shock front has a characteristic coherence length $\lambda_B \sim c/\omega_p \sim 10^7$cm. For such a short coherence length, the field is expected to dissipate over several tens of c/ω_p behind the shock. However, in order to account for the observations, the entire shocked shell, the thickness of which is $\Delta' \sim R/\Gamma \sim \Gamma ct \sim 10^{17}$cm, should be emitting synch. radiation. The survival of the field over $\sim 10^{10} c/\omega_p$ is a major challenge to the theory. It probably implies that λ_B increases by orders of mag. @ downstream, via some non-linear process related to the generation of high energy particles.

Two comments are in place here.

1. One may suggest that large coherence length of a pre-existing B field in the upstream may lead to large scale field in the downstream. However, in the ISM the magnetic field carries a fraction $\sim 10^{-9}$ of the plasma rest mass energy density, which implies, for a relativistic shock, that B carries 10^{-9} of the energy influx into the shock (while it should carry ~0.1 of the energy flux in the downstream). In this case, it is likely that the upstream field plays no role in the shock structure.
2. Numerical plasma simulations show the generation of a shock wave of thickness $\sim 10\ c/\omega_p$ as expected. However 3D simulations are limited to transverse (i.e. perpendicular to shock velocity direction) size of $\sim 50\ c/\omega_p$ and can not therefore address the problem of λ_B increase by orders of mag. and particle acceleration to UHE.

GRBs- Summary

* Prompt emission: most likely internal dissipation within a highly relativistic wind driven by mass accretion onto newly formed few solar mass BH.

  Models where the wind energy flux is dominated by plasma kinetic energy may naturally account for the dissipation and emission of MeV photons, as synch. emission of electrons accelerated in collisionless shocks. See fig. 6.

* The constraints on the properties of GRB sources, implied by 1—100 MeV observations, are similar to the constraints, derived from independent observations and arguments, that should be satisfied by the sources of UHECRs. See table 1.

* Afterglow emission: most likely produced by synch. emission of electrons accelerated by a collisionless shock driven into the surrounding medium.

  The dynamics of the model is well understood theoretically, and was stringently (and successfully) tested by observations.

GRBs- Open Q's

* Collapsing object- beyond the scope of these lectures.
* Jet generation/acceleration mechanism,
  dominant jet energy flux (EM/Kinetic).
  jet entrainment mass $<10^{-6}\ M_{sun}$.
* Energy dissipation and radiation emission mechanisms,
  The physics of collisionless shocks: e^- coupling, B survival.
* Acceleration to UHE?

Potential contributions of GLAST

GLAST will cover the yet unobserved range of 30MeV—300GeV. It may therefore provide important new constraints on the prompt emission mechanism, on the Lorentz factor Γ and on the environment density.

Note, that due to the weak dependence of the Γ constraint (IIa.2) on the max. observed photon energy, detection of pair production optical depth effects is not guaranteed.

III. Large scale structure (LSS) shocks

* Most of the baryons in the present day universe are believed to be contained in ~1Mpc diameter filaments, which occupy ~0.1 of the volume and where the plasma density is ~10 times the universal average. The plasma collapsed due to the growth of gravitational instabilities. The characteristic collapse velocity is ~3Mpc/t_H ~3×10^7cm/s. This kinetic energy of the infalling plasma is converted to thermal energy by a collisionless shock, $T\sim[(\Gamma-1)/(\Gamma+1)^2]m_p v^2$=0.1keV (here Γ=5/3 is the adiabatic index of the gas).

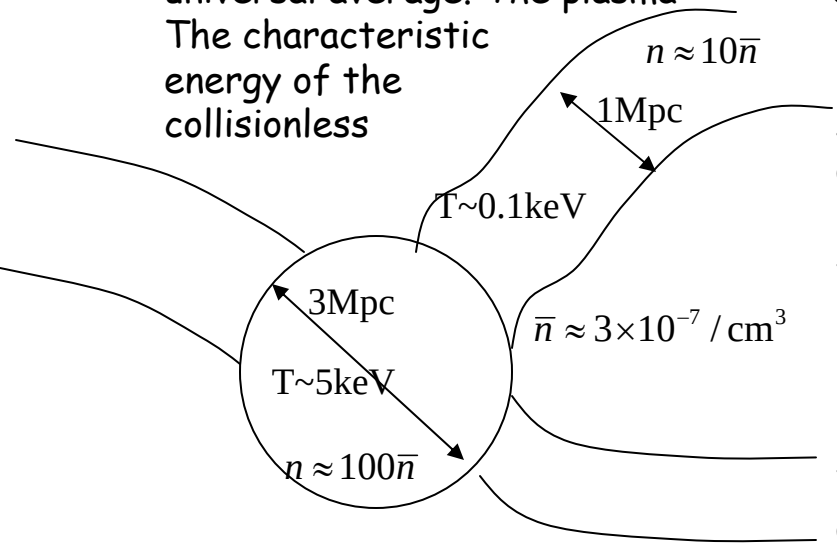

* A small fraction of the plasma is concentrated in clusters, where the density and temperature are higher (100 times the universal average density, few keV).

* The magnetic field in the filaments may be estimated by assuming that the field built in the collisionless shock (see IIb) carries a significant fraction ε_B of the thermal energy density, $B=(8\pi\varepsilon_B nT)^{1/2}\sim0.01(\varepsilon_B/0.01)^{1/2}\mu G$. The value ε_B=0.01 is chosen since it reproduces the observed ~0.1μG fields in cluster halos.

* As we have shown (I.3), proton acceleration is limited to energy $E_p<(v/c)eBR$ which yields ~10^{16}eV for the filaments and ~3×10^{18}eV for the clusters.

* The acceleration of electrons by LSS shocks is limited by energy losses due to IC scattering of CMB photons. As discussed in Drury's lectures, the acceleration time to energy E in a collisionless shock of velocity v=βc is ~$R_L/\beta^2 c$ where the Larmor radius is E/eBc. This gives

  $t_{acc}=10^{-3}\,\gamma_e$ yr for acceleration to $E=\gamma_e m_e c^2$. The energy loss time is given by E/P_{IC}, where $P_{IC}=\sigma_T c\,\gamma_e^2 u_{CMB}$. This yields

  $t_{IC}=10^{12}\,\gamma_e^{-1}$ yr. Comparing t_{IC} and t_{acc} we find that the maximum electron energy is $\gamma_{e,max}=3\times10^7$ yr.

* Electrons with $\gamma_e>\gamma_c$=100 cool by IC over t_H. Thus, the energy deposited in shock accelerated

electrons is converted to non-thermal radiation. Assuming that the electron spectrum follows $\gamma_e^2 dn_e/d\gamma_e \sim$Const, as expected for collisionless shock acceleration, the radiation spectrum will extend as $E_\gamma^2(dn_\gamma/dE_\gamma)$=Const from $\sim\gamma_c^2 3T_{CMB}\sim$100eV to $\sim\gamma^2_{e,max}3T_{CMB}\sim$1TeV. Assuming that a fraction η_e of the thermal shocked plasma energy is carried by accelerated electrons, the energy density of this radiation would be $\sim\eta_e\langle n\rangle T$ and the energy flux is expected to be

$$E_\gamma^2 dJ/dE_\gamma \approx \frac{c}{4\pi}\frac{\eta_e \bar{n} T}{\ln(\gamma^2_{e,\max})} \approx 0.1\frac{\eta_e}{0.05}\frac{\text{keV}}{\text{cm}^2\text{s sr}} \quad , \quad E_\gamma < 1\text{TeV}.$$

we have chosen here $\eta_e\sim$0.05, as derived from observations of SNR shocks (which have similar velocities). This flux is ~10% of the extra-Galactic flux reported by EGRET. Note, however, that the flux derived by EGRET's team is most likely only an upper limit on the extra-Galactic flux (the intensity is dominated by the Galactic component, and the intensity obtained after subtracting a Galactic model is still correlated with Galactic structures; See Keshet, Waxman & Loeb 2004 for discussion).

* Clusters are expected to emit high energy non-thermal radiation by a similar process- IC cooling of electrons accelerated in the cluster accretion shock. The gas accretion rate of the cluster may be estimated as $\sim M_g/t_v$, where M_g is the baryonic cluster mass and $t_v=t_H/3$ is the virialization time, and L_{IC} by $L_{IC}\sim (M_g/m_p t_H)\,\eta_e T$. Thus, we expect

$$E_\gamma^2 df/dE_\gamma \approx \frac{M_g}{m_p t_H/3}\frac{\eta_e T}{\ln(\gamma^2_{e,\max})} \approx 10^{43.5}\frac{M_g}{10^{14}M_{\text{sun}}}\frac{\eta_e}{0.05}\frac{T}{10\text{keV}}\,\text{erg/s} \quad , \quad E_\gamma < 1\text{TeV}.$$

* High energy non-thermal emission is also expected from the decay of pions produced by inelastic pp interactions of cosmic-ray protons accelerated in the shocks with cluster gas. The fraction of proton energy f_p lost to such interaction is given by the product of the interaction rate, $n\sigma_{pp}c$, t_H and the fractional energy loss per interaction, $\sim m_\pi/m_p$. For $n=100\langle n\rangle$, σ_{pp}=30mb we have f_p=0.001. The fraction of energy converted to photons is $\sim f_p/2=5\times10^{-4}$. Protons residing at the cores of massive clusters may lose a higher fraction of their energy since the density is higher there, $n\sim10^{-3}$/cc leading to $f_p/2=1.5\times10^{-2}$. However, since only ~0.1 of the protons are at the core,

the average fraction of proton energy lost to high energy gamma-ray production is ~0.001. Thus, the IC flux is expected to be dominated by the electrons by a factor of $1000(\eta_e/\eta_p)$, where η_p is the fraction of thermal shocked plasma energy carried by accelerated protons.

* The non-thermal IC accretion shock emission described above may have already been observed in the Coma cluster, as illustrated in fig. 8. The high energy emission detected by Integral is consisted with the prediction of the accretion shock model described above. The lack of correlation between the high energy emission and the thermal emission is consistent with the hypothesis that the emission is due to IC from electrons accelerated at the shock, and inconsistent with decay of pions produced in pp collisions. As indicated in the fig., the prdicted flux should be easily detectable by GLAST.

Fig. 8 [from D. Kushnir]: First Detection of Accretion Shock in Coma ?

INTEGRAL : 44-107 keV

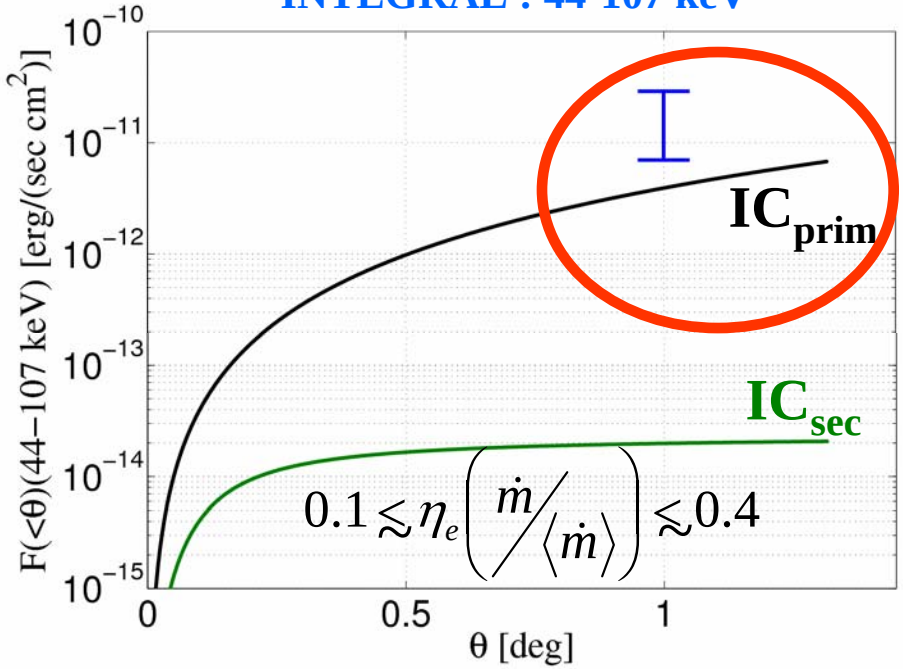

EGRET : > 100 MeV

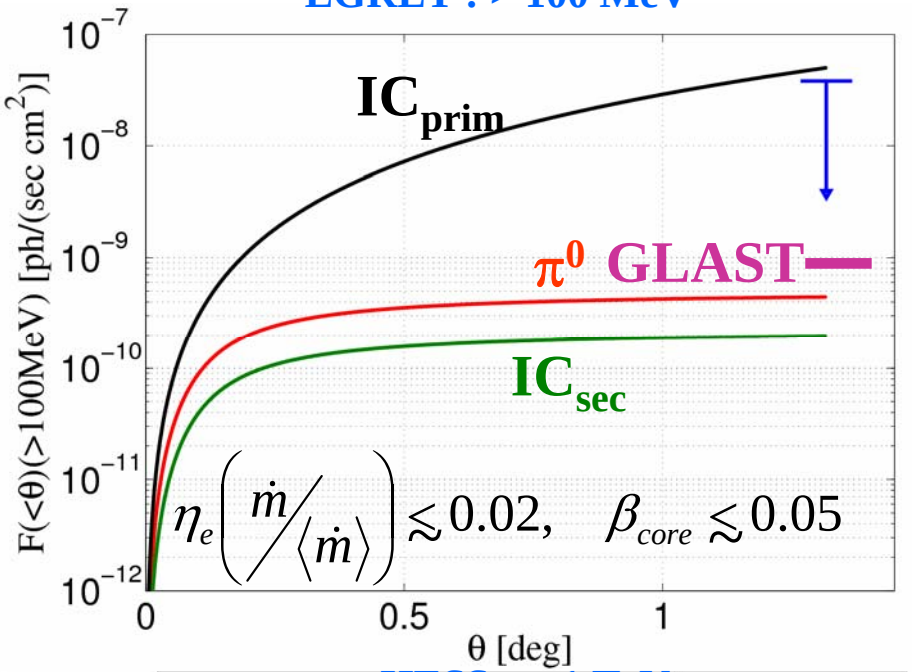

No correlation with thermal

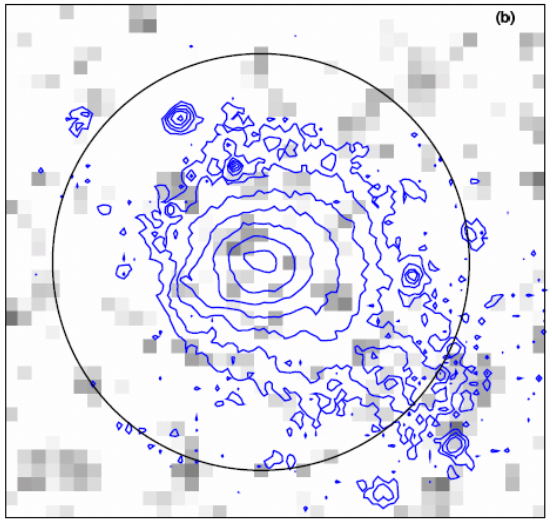

HESS : > 1 TeV

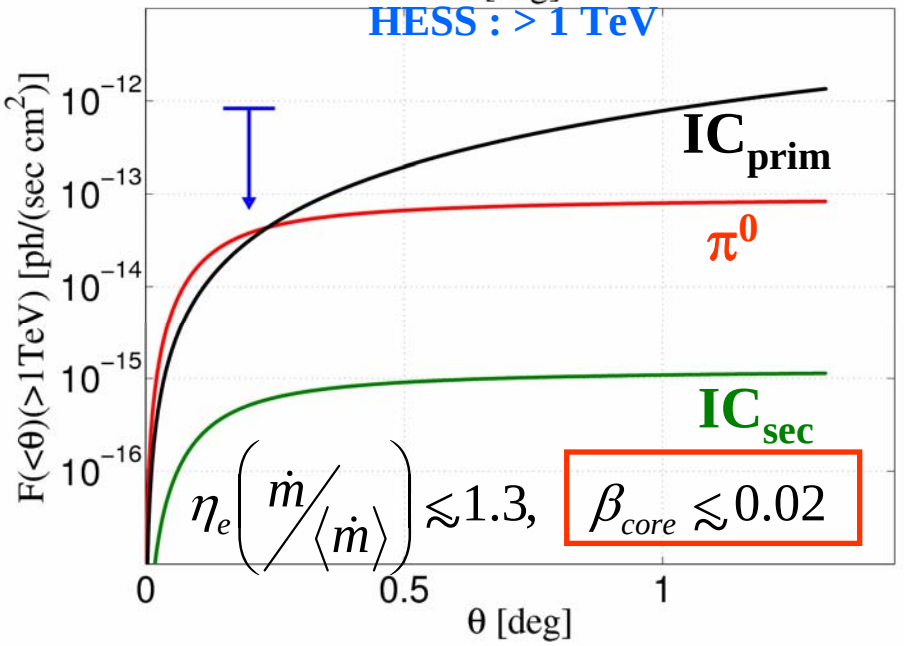

LSS shocks- Summary and predictions for HE gamma-ray observations

* The universe is predicted to be filled with diffuse high energy radiation produced by electrons accelerated in LSS shocks,

$$\mathrm{E}_\gamma^2 dJ/dE_\gamma \approx 0.1 \frac{\eta_e}{0.05} \frac{\mathrm{keV}}{\mathrm{cm}^2 \mathrm{s\ sr}} \quad , \quad E_\gamma < 1\mathrm{TeV}.$$

The intensity should show some weak anisotropy, correlated with extra-Galactic radio emission.

* High energy emission from clusters of galaxies is predicted to be dominated by IC emission of electrons accelerated in the accretion shocks. The predicted luminosity is

$$\mathrm{E}_\gamma^2 df/dE_\gamma \approx 10^{43.5} \frac{M_g}{10^{14} M_{\mathrm{sun}}} \frac{\eta_e}{0.05} \frac{T}{10\mathrm{keV}} \mathrm{erg/s} \quad , \quad E_\gamma < 1\mathrm{TeV}.$$

The predicted emission may have already been observed in Coma, and should be detected by GLAST.

GLAST should detect ~$10^{1.5}$ clusters with f(>100MeV)>10^{-9}/cm^{2}s. The nearest objects may be detectable by higher energy instruments (HESS, Magic, Veritas).